Design for a spin-Seebeck diode based on two-dimensional materials

Hua-Hua Fu,[1,*] Dan-Dan Wu,[1] Lei Gu,[1] Menghao Wu,[1] and Ruqian Wu[2,†]

[1]*College of Physics and Wuhan National High Magnetic Field Center, Huazhong University of Science and Technology,*
Wuhan 430074, People's Republic of China
[2]*Department of Physics and Astronomy, University of California, Irvine, California 92697-4575, USA*

Studies of the spin-Seebeck effect (SSE) are very important for the development of fundamental science and novel low-power-consumption technologies. The spin-Seebeck diode (SSD), in which the spin current can be driven by a forward temperature gradient but not by a reverse temperature gradient, is a key unit in spin caloritronic devices. Here, we propose a SSD design using two-dimensional (2D) materials such as silicene and phosphorene nanoribbons as the source and drain. Due to their unique band structures and magnetic states, thermally driven spin-up and spin-down currents flow in opposite directions. This mechanism is different from that of the previous one, which uses two permalloy circular disks [Phys. Rev. Lett. **112**, 047203 (2014)], and the SSD in our design can be easily integrated with gate voltage control. Since the concept of this design is rather general and applicable to many 2D materials, it is promising for the realization and exploitation of SSDs in nanodevices.

I. INTRODUCTION

Spin caloritronics examines the relationship between spin and heat transport in materials, and it may offer additional possibilities for thermoelectric waste heat recovery [1,2] and information-processing technologies [3–6]. A legendary discovery of spin caloritronics research is the observation of the spin-Seebeck effect (SSE) [7], in which a spin current and an associated spin voltage are induced by a temperature gradient. As a further step toward device applications, a design of a spin-Seebeck diode (SSD) was proposed in a spin-valve nanopillar geometry that allows the thermal-induced spin current to flow only in one direction [8]. Its physical mechanism relies mainly on the spin-wave excitations at metal-magnetic insulator interfaces, which is certainly not the only route to realize the SSE [2]. For high performance and easy control, it is desired to exploit the momentum-spin lock features of two-dimensional (2D) materials [9–11] for the design of a SSD; the principles of such a design have not been established yet.

In this work, we demonstrate the possibility of making an additional SSD for spin caloritronics devices based on 2D materials, in which the microscopic mechanism is different from the previous one [8]. We adopt a zigzag silicene nanoribbon (ZSiNR) heterojunction in our design to elucidate the concept. Silicene, a realistic monolayer of silicon atoms bonded together in a 2D honeycomb lattice such as graphene, was synthesized very recently [12,13]. The electronic structure of silicene from *ab initio* calculations is similar to that of graphene [14] in that both have high electric conductivity. However, silicene is not strictly planar, but it has a buckled structure with a height difference Δ between adjacent Si atoms of about 0.46 Å [15,16], which leads to a nonzero energy gap and remarkably enhances the Seebeck coefficient [17,18]. To realize a SSD, we need to have magnetic ZSiNR, which typically can be done through doping [19], defects [20], and

edge modification [21]. Here, we use hydrogen-terminated ZSiNR, which can be fabricated by controlling the chemical potential of hydrogen via the temperature and pressure of H_2 gas [22,23]. More explicitly, the ZSiNR heterojunction in our SSD design has a double-hydrogen-terminated ZSiNR (N-ZSiNR-H_2, sp^3-hybrid) as the source and a single-hydrogen-terminated ZSiNR (N-ZSiNR-H, sp^2-hybrid) as the drain [see Fig. 1(a)], where N denotes the number of zigzag Si chains across ZSiNR. We focus on the spin currents driven by temperature difference, ΔT, between the source temperature T_L and the drain temperature T_R. Our calculations demonstrated that (i) by applying a temperature gradient between two contacts, spin-dependent currents with opposite spin directions are driven in the device and just flow in opposite directions; (ii) due to the special band structures and magnetic states, the spin current can be driven by a forward temperature gradient but not by a reverse temperature gradient, indicating that the SSD behavior appears in the device; (iii) the SSD in our device designs can be easily integrated with gate voltage control; and (iv) the concept of the device design is rather general and can be extended to other 2D materials, such as zigzag phosphorene nanoribbons.

The remainder of this paper is organized as follows. In Sec. II, theory and computational details are described. In Sec. III, we present the calculated results of the SSD effect in ZSiNRs, discuss its physical mechanism, explore the influences of a wide nanoribbon and gate voltage on the SSD, and then extend the design concept to other 2D materials. Finally, a short summary is given in Sec. IV.

II. THEORY AND METHOD

Our calculations were performed using density-functional theory (DFT) and the nonequilibrium Green's-function technique [24,25]. Geometry optimization and electronic structure calculations were first carried out with the SIESTA code [26]. The positions of all the atoms were relaxed until the maximum force on them was less than 0.01 eV/Å. We then calculated the transmittances across the ZSiNR heterojunction with the TRANSIESTA code [27,28]. The core electrons

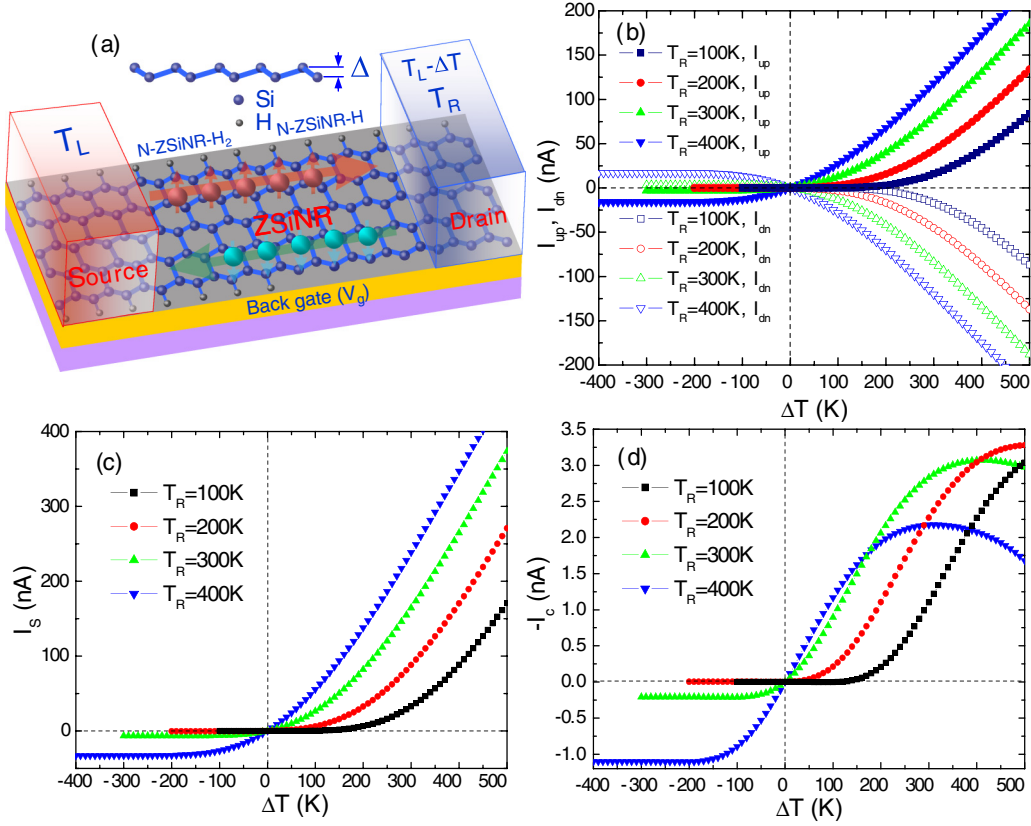---

*hhfu@hust.edu.cn
†wur@uci.edu

FIG. 1. (Color online) (a) Schematic of the ZSiNR-heterojunction-based spin caloritronics device, where the ZSiNR heterojunction is composed of N-ZSiNR-H$_2$ (source) and N-ZSiNR-H (drain) and placed on a substrate with a gate voltage. ΔT represents the temperature difference between the source (T_L) and the drain (T_R), i.e., $T_L - T_R$. (b) Spin-dependent currents I_{up} and I_{dn} vs ΔT; their opposite signs indicate that they flow in opposite directions. (c) The total spin current I_s ($= I_{up} - I_{dn}$) and (d) the net electronic current I_c ($= I_{up} + I_{dn}$) in the 4-ZSiNR heterojunction vs ΔT for some chosen values of T_R (here, $-I_c$ is plotted since $|I_{dn}| > I_{up}$ in a large region of ΔT).

were described by norm-conserving pseudopotentials, and the Perdew-Burke-Ernzerhof functional of the generalized gradient approximation was adopted for the description of the exchange-correlation interactions among electrons [29]. The double-zeta plus polarization basis set with an energy cutoff of 150 Ry and a Monkhorst-Pack k-mesh of $1\times1\times100$ in the Brillouin zone were chosen in our calculations.

In the Landauer-Büttiker formalism, the spin-dependent current through the device is given by $I_\sigma = \frac{e}{h} \int_{-\infty}^{\infty} \{T_\sigma(E) [f_L(E,T_L) - f_R(E,T_R)]\} dE$ [30], where e is the electron charge and h is the Planck constant, $f_{L(R)}(E,T_{L(R)})$ is the equilibrium Fermi-Dirac distribution for the source (drain), and $T_\sigma(E)$ is the spin-resolved transmittance function, which is defined as $T_\sigma(E) = \text{Tr}[\Gamma_L G_\sigma^R \Gamma_R G_\sigma^A]$ [29], where $G_\sigma^{R(A)}$ is the retarded (advanced) Green's functions of the scattering region, σ ($=\uparrow, \downarrow$) denotes the spin index, and $\Gamma_{L(R)}$ is the coupling matrix of the source (drain). These expressions will help us to obtain the thermal spin-dependent transport through the ZSiNR heterojunctions.

III. RESULTS AND DISCUSSION

Figure 1(b) gives the calculated spin currents of the 4-ZSiNR heterojunction versus ΔT for various T_R. It is clear that the spin-dependent currents are generated in this structure without the need for the electric field or the gate voltage.

Since the spin-up current I_{up} is positive and the spin-down current I_{dn} is negative, i.e., they flow in opposite directions
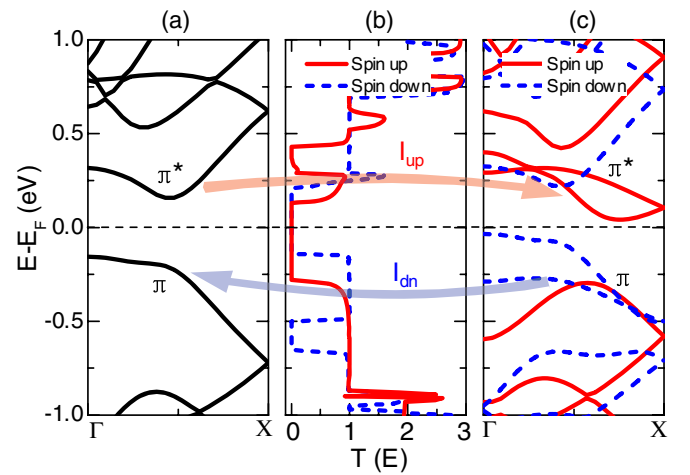

FIG. 2. (Color online) Parts (a) and (c) show the band structures of the source 4-ZSiNR-H$_2$ and the drain 4-ZSiNR-H, and (b) (middle panel) shows the spin-resolved transmission spectra of the 4-ZSiNR heterojunction. The red arrow (blue arrow) illustrates the flowing direction of the spin-up (spin-down) current, where the transmission is united by e^2/h.

with approximately equal magnitudes, the SSE in the ZSiNR heterojunction is nearly perfect.

Strikingly, both I_{up} and I_{dn} are asymmetric about the zero point of ΔT. For $\Delta T < 0$, that is, $T_L < T_R$, both I_{up} and I_{dn} remain zero when $T_R \leqslant 300$ K. For $\Delta T > 0$, both I_{up} and I_{dn} increase sharply after a threshold temperature difference, ΔT_{th}. In particular, ΔT_{th} decreases to zero as T_R increases. Since our main purpose is to design SSD in nanodevices, we plot the total spin current I_s ($= I_{up} - I_{dn}$) and the net electron currents I_c ($= I_{up} + I_{dn}$) versus ΔT for different values of T_R in Figs. 1(c) and 1(d), respectively. The spin current shows an excellent diode feature for $T_R \leqslant 300$ K, allowing the thermal-induced spin currents to flow in one direction only. Even for high T_R, e.g., $T_R = 400$ K, the ZSiNR heterojunction still behaves as a robust spin-Seebeck rectifier (SSR) since I_s in the negative ΔT side is significantly smaller than that in the positive ΔT side. Moreover, the values of I_s [see Fig. 1(d)] are nearly two orders of magnitude larger than those of I_c in the entire ranges of ΔT and T_R, indicating the carrier transport in this structure is dominated by the spin current. This ensures the high performance and low energy consumption of our SSD design.

In addition, I_c also displays a thermoelectric diode and rectifier behaviors, and it shows a negative differential thermoelectric resistance (NDTR), which originates from the competition between I_{up} and I_{dn} with opposite flowing directions.

To understand the SSD behavior of the junction, we present the band structures of the two terminals and its spin-resolved transmission in Fig. 2. Our first-principles calculations indicate that the left panel, 4-ZSiNR-H_2, has an antiferromagnetic ground state, while the right panel, 4-ZSiNR-H, has a ferromagnetic one, which is consistent with their previous magnetism studies [31]. From the band structures shown in Figs. 2(a) and 2(c), one can find that only their bonding π bands and antibonding π^* bands are near the Fermi level. In particular, these states in the source are degenerated in spin while they have spin splitting in the drain. Such a unique combination of bands gives rise to the spin-resolved transmission spectrum of the junction and subsequently its SSD feature discussed above. As shown in Fig. 2(b), the transmission peaks for the spin-up and spin-down electrons are in different energy regions, i.e., $0.13 < (E - E_F) < 0.36$ eV for spin-up and $-0.5 < (E - E_F) < -0.14$ eV for spin-down,
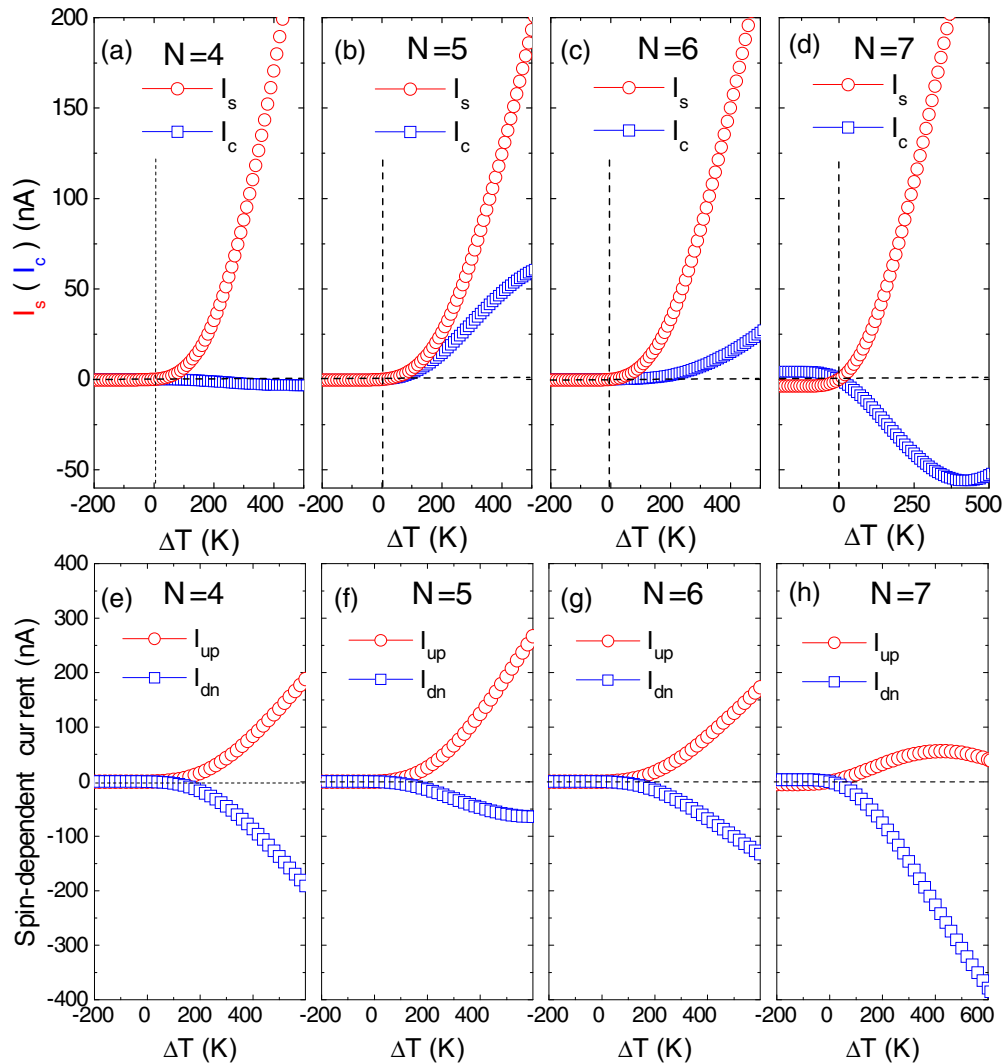

FIG. 3. (Color online) (a)–(d) The total spin current I_s and the net electron current I_c as a function of ΔT for various N-ZSiNR heterojunctions with $N = 4$–7 and $T_R = 200$ K. (e) and (f) The corresponding spin-up currents I_{up} and spin-down currents I_{dn} vs ΔT.

respectively. This breaks the electron-hole symmetry and leads to nonzero net spin currents. More explicitly, the main transmission peak for the spin-up channel is above the Fermi level; positive spin-up current is produced by electron transport from the source to the drain at sufficiently high T_L. In contrast, the major transmission peak for the spin-down channel is below the Fermi level, and the flow of holes from the source to the drain causes a negative spin-down current. The similar amplitudes of $T_{\rm up}$ and $T_{\rm dn}$ near the Fermi level lead to nearly equal magnitudes of $I_{\rm up}$ and $I_{\rm dn}$. Since the band gap of the source is much larger than that of the drain, the transport channels open only when $\Delta T > 0$, which leads to the SSD feature of the junction. It is clear that the physical mechanism to realize SSD here is different from the previous one based on the spin-wave excitations in the metal-insulator interface [8].

Obviously, the operation ΔT, T_R as well as the spin filtering efficiency of our SSD depends on the band gaps of the source and drain. The band gap of a nanoribbon opens because of the interaction between two edges, and it is hence useful to examine the effect of the width of ZSiNRs on the performance of SSD. Figures 3(a)–3(d) show I_s and I_c versus ΔT for the N-ZSiNR heterojunction with $N = 4$–7. It is clear that the SSD feature stays in wider ZSiNRs especially when N is even. For odd-N cases, $I_{\rm up}$ and $I_{\rm dn}$ have much different amplitudes and I_c is no longer negligible. Obviously, the geometrical symmetry

and the width play important roles in the spin caloritronics of ZSiNR since they lead to different gaps and transmission probabilities between the π and π^* states [31].

Furthermore, the band gaps and band alignments of ZSiNRs can be tuned by applying a back gate voltage (V_g). To illustrate this point, we take the 5-ZSiNR heterojunction as an example, and we plot the curves of I_s and I_c versus ΔT for various V_g in Figs. 4(a1)–4(e1). While negative V_g raises I_c [see Fig. 4(a1)], positive V_g can efficiently suppress I_c without scarifying I_s. As V_g increases to 1.25 V, I_c is reduced to zero in a wide range of ΔT, indicating the nearly perfect SSD feature even in the 5-ZSiNR heterojunction. We found that the increase of V_g lowers $I_{\rm up}$ and raises $I_{\rm dn}$, and as V_g increases to the critical value 1.25 V, the curve of $I_{\rm up}$ is nearly symmetric to that of $I_{\rm dn}$. To shed some light on the mechanism of the V_g dependence of I_c, we plot the spin-resolved transmission $T_{\rm up,dn}(E)$ under various gate voltages in Figs. 4(a2)–4(e2). In the insets, the spin-down hole transmittance ($E < E_F$) is flipped to the positive energy side for ease of comparison with the spin-up electron transmittance ($E > E_F$). For negative V_g [see Fig. 4(a2)], $T_{\rm dn}$ starts from a larger energy and has a lower amplitude than that of $T_{\rm up}$, and hence we have $I_{\rm up} > |I_{\rm dn}|$ and a net I_c. For positive V_g, $T_{\rm up}$ is gradually suppressed near the Fermi level, whereas $T_{\rm dn}$ remains unchanged. As a result, I_c decreases to zero because of the cancellation between $I_{\rm up}$ and
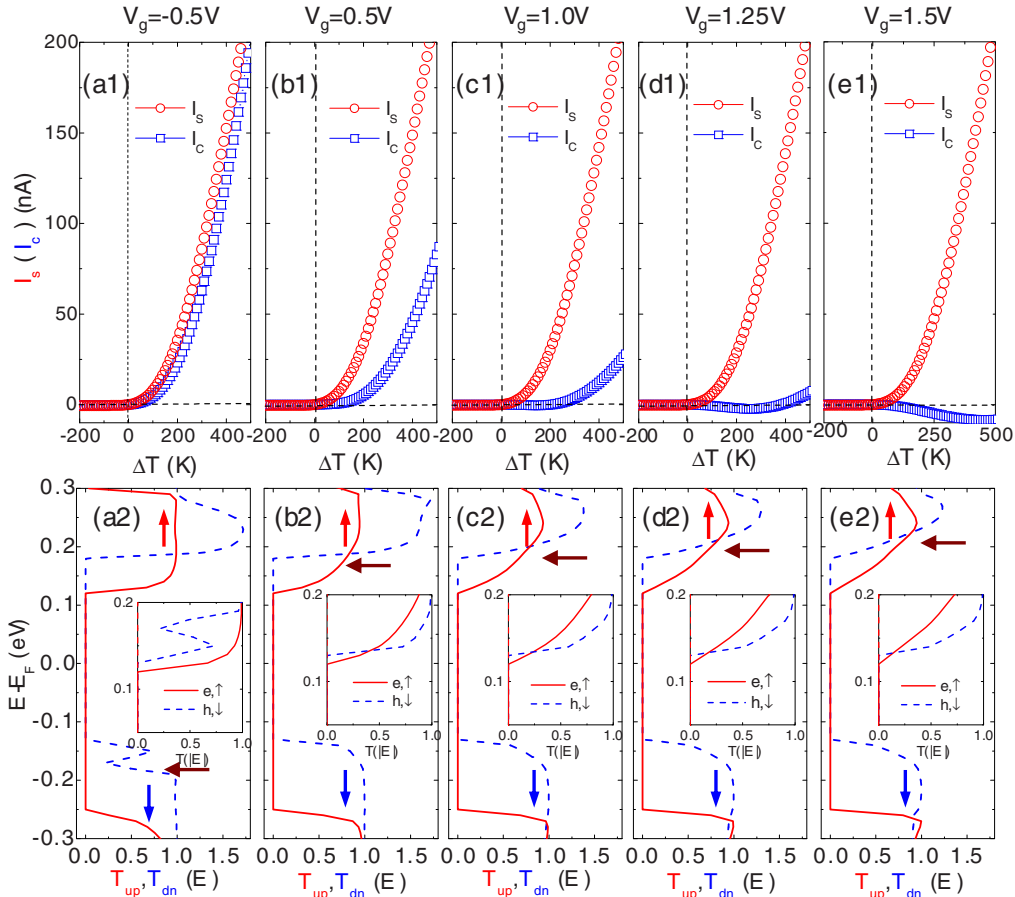

FIG. 4. (Color online) (a1)–(e1) The total spin current I_s and the net electron current I_c vs ΔT in the 5-ZSiNR heterojunction for gate voltage $V_g = -0.5$, 0.5, 1.0, 1.25, and 1.5 V, respectively. Parts (a2)–(e2) show the corresponding spin-resolved transmission spectra $T_{\rm up}$ and $T_{\rm dn}$ (E) for electrons ($E > E_F$) and holes ($E < E_F$) near the Fermi level.

I_{dn}. As V_g increases further, for example $V_g = 1.5$ V, T_{up} is suppressed further and I_{dn} overtakes I_{up}, leading to a negative I_c. Apparently, the gate voltage is an effective parameter to reduce the conducting charge currents and optimize the SSD performance of the ZSiNR heterojunctions.

Apparently, our SSD design is applicable to junctions of many two-dimensional materials as long as they have appropriate magnetic states, band gaps, and band alignments. Here we show that the SSD feature can also be realized at the junctions of phosphorene nanoribbons. Phosphorene is a 2D material possessing a honeycomb structure of black

phosphorus. Just as graphene can be isolated by peeling graphite, phosphorene can be similarly isolated from black phosphorus by the mechanical exfoliation method [32–34], and it seems to be more stable than silicene [34]. It is reported that phosphorene nanoribbons can be optimized to have superb thermoelectric performance even at room temperatures [35]. Following the design in Fig. 1(a), we use the pristine zigzag phosphorus nanoribbon (ZPNR) as the source and the single-hydrogen-terminated ZPNR (ZPNR-H) as the drain, as illustrated in Fig. 5(a), where a similar ΔT ($=T_L - T_R$) is applied between the source and the drain. The first-principles calculations show that the pristine 4-ZPNR has an antiferromagnetic ground state [see Fig. 5(b)], while the 4-ZPNR-H has a ferromagnetic one [see Fig. 5(d)], in agreement with the previous magnetic analysis for the ZPNRs [36]. The band structures of the source and the drain give nearly symmetric spin-dependent transmission spectra, as shown in Fig. 5(c). As a result, the spin-up current I_{up} flows from the drain to the source, while the spin-down current I_{dn} flows in the opposite direction, as illustrated in Fig. 5(c). The opposite flows of I_{up} and I_{up} nearly cancel the charge current. Again, the curves of I_s versus ΔT display good SSD feature in Fig. 5(e) due to the larger band gap of the source. As the band gap decreases for wider ZPNRs, the value of ΔT_{th} also decreases and the SSD behavior remains, as shown in Fig. 5(f), where the spin currents for the 7-ZPNR heterojunction are plotted. This phenomenon can be used for the reduction of ΔT to a practical range for device operations. Moreover, very recent studies showed that external electric field [37] and compressive strain [38,39] are also effective to control the band gaps of ZPNRs. Thus we can integrate and manipulate the operation of the ZPNR-based SSDs with other means, as desired for sensing, spintronics, and spin caloritronics applications.

IV. SUMMARY

In conclusion, we have proposed a design concept for making SSD with a ZSiNR heterojunction. Spin-dependent currents can be generated in the device by using the temperature gradient instead of the external electric bias. Appropriate control on the magnetic states and band structures of the source and drain allow almost perfect cancellation between thermal-induced spin-up and spin-down currents that flow in opposite directions with nearly equal magnitudes across the heterojunction. The SSD is realized because of the difference in band gaps between the source and drain. The SSD obtained here shows an odd-even symmetry; the even-N ZSiNR is beneficial as a good SSD, while the odd-N ZSiNR tends to generate a high-polarized spin current. Moreover, we found that the gate voltage is an effective parameter to reduce conducting charge currents and optimize the SSD performance of the ZSiNR heterojunctions. More importantly, the design concept of the SSD is rather general and can be extended to other 2D materials, such as the ZNPRs with appropriate magnetic states, band gaps, and band alignments. In addition, the performance of ZSiNR- and ZPNR-based SSDs can be conveniently tuned by adjusting their widths and compressive stain. Our design principles provide a strategy for the realization of SSD or other tunable spintronics nanodevices.
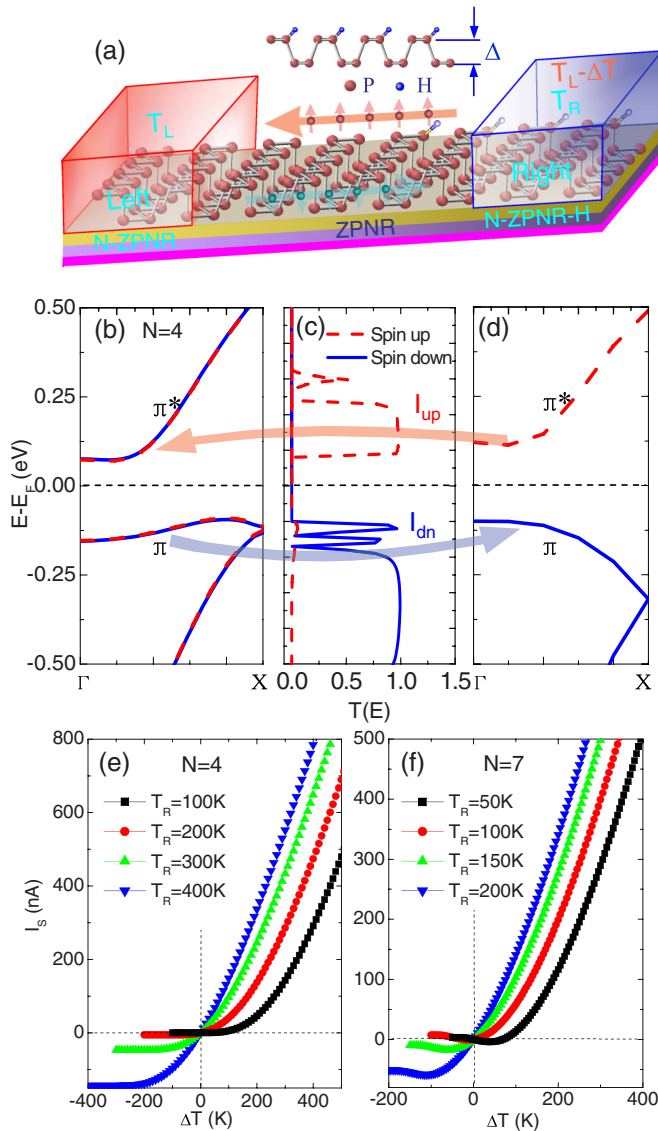
FIG. 5. (Color online) (a) Schematic illustration of a zigzag phosphorene-nanoribbon (ZPNR)-based spin caloritronics device. The ZPNR nanoribbon heterojunction is composed of antiferromagnetic N-ZPNR as the source and ferromagnetic single-hydrogen-terminated N-ZPNR (N-ZPNR-H) as the drain. (b) and (d) The band structures of the source 4-ZPNR and the drain 4-ZPNR-H. (c) The spin-dependent transmission spectra in the 4-ZPNR heterojunction. (e) and (f) The spin currents I_s vs the device temperature difference ΔT ($=T_L - T_R$) in the 4-ZPNR heterojunction and the 7-ZPNR one, respectively. It clearly shows that SSD appears in both devices.

[1] S. T. B. Goennenwein and G. E. W. Bauer, Nat. Nanotechnol. **7**, 145 (2012).

[2] G. E. Bauer, E. Saitoh, and B. J. van Wees, Nat. Mater. **11**, 391 (2012).

[3] P. H. Chang, M. S. Bahramy, N. Nagaosa, and B. K. Nikolić, Nano Lett. **14**, 3779 (2014).

[4] J. Nakabayashi, D. Yamamoto, and S. Kurihara, Phys. Rev. Lett. **102**, 066803 (2009).

[5] W. Y. Kim and K. S. Kim, Nat. Nanotechnol. **3**, 408 (2008).

[6] K. R. Jeon, B. C. Min, A. Spiesser, H. Saito, S. C. Shin, S. Yuasa, and R. Jansen, Nat. Mater. **13**, 360 (2014).

[7] K. Uchida, S. Takahashi, K. Harii, J. Ieda, W. Koshibae, K. Ando, S. Maekaea, and E. Saitoh, Nature (London) **455**, 778 (2008).

[8] S. Borlenghi, W. Wang, H. Fangohr, L. Bergqvist, and A. Delin, Phys. Rev. Lett. **112**, 047203 (2014).

[9] M. Zeng, Y. Feng, and G. Liang, Nano Lett. **11**, 1369 (2011).

[10] T. Kuschel and G. Reiss, Nat. Nanotechnol. **10**, 22 (2015).

[11] H. Adachi, K. Uchida, E. Saitoh, and S. Maekawa, Rep. Prog. Phys. **76**, 036501 (2013).

[12] B. Lalmi, H. Oughaddou, H. Enriquez, A. Kara, S. Vizzini, B. Ealet, and B. Aufray, Appl. Phys. Lett. **97**, 223109 (2010).

[13] P. Vogt, P. De Padova, C. Quaresima, J. Avila, E. Frantzeskakis, M. C. Asensio, A. Resta, B. Ealet, and G. Le Lay, Phys. Rev. Lett. **108**, 155501 (2012).

[14] S. Lebègue and O. Eriksson, Phys. Rev. B **79**, 115409 (2009).

[15] Z. Y. Ni, Q. H. Liu, K. C. Tang, J. X. Zheng, J. Zhou, R. Qin, Z. X. Gao, D. P. Yu, and J. Lu, Nano Lett. **12**, 113 (2012).

[16] N. D. Drummond, V. Zólyomi, and V. I. Fałko, Phys. Rev. B **85**, 075423 (2012).

[17] K. Zberecki, M. Wierzbicki, J. Barnaś, and R. Swirkowicz, Phys. Rev. B **88**, 115404 (2013).

[18] X. L. Zhang, H. Xie, M. Hu, H. Bao, S. Y. Yue, G. Z. Qin, and G. Su, Phys. Rev. B **89**, 054310 (2014).

[19] Y. Li, Z. Zhou, and P. Shen, ACS Nano **3**, 1952 (2009).

[20] X. Lin and J. Ni, Phys. Rev. B **84**, 075461 (2011).

[21] E. J. Kan, Z. Li, J. Yang, and J. G. Hou, J. Am. Chem. Soc. **130**, 4224 (2008).

[22] T. Wassmann, A. P. Seitsonen, A. M. Saitta, M. Lazzeri, and F. Mauri, Phys. Rev. Lett. **101**, 096402 (2008).

[23] R. Jansen, Nat. Mater. **11**, 400 (2012).

[24] H. H. Fu and K. L. Yao, J. Chem. Phys. **134**, 054903 (2011).

[25] H. H. Fu and K. L. Yao, Appl. Phys. Lett. **100**, 013502 (2012).

[26] J. M. Soler, E. Artacho, J. D. Gale, A. Garcia, J. Junquera, P. Ordejon, and D. Sanchez-Portal, J. Phys.: Condens. Matter **14**, 2745 (2002).

[27] J. Taylor, H. Guo, and J. Wang, Phys. Rev. B **63**, 245407 (2001).

[28] J. E. Padilha, M. P. Lima, A. J. R. da Silva, and A. Fazzio, Phys. Rev. B **84**, 113412 (2011).

[29] J. P. Perdew, K. Burke, and M. Ernzerhof, Phys. Rev. Lett. **77**, 3865 (1996).

[30] Y. Imry and R. Landauer, Rev. Mod. Phys. **71**, S306 (1999).

[31] J. Kang, F. Wu, and J. Li, Appl. Phys. Lett. **100**, 233122 (2012).

[32] L. Li, Y. Yu, G. J. Ye, Q. Ge, X. Ou, D. Feng, X. H. Chen, and Y. Zhang, Nat. Nanotechnol. **9**, 372 (2014).

[33] E. S. Reich, Nature **506**, 19 (2014).

[34] H. Liu, A. T. Neal, Z. Zhu, X. Xu, K. Tomanek, and P. D. Ye, ACS Nano **8**, 4033 (2014).

[35] R. X. Fei, A. Faghaninia, R. Soklaski, J. A. Yan, C. Lo, and L. Yang, Nano Lett. **14**, 6393 (2014).

[36] Z. Zhu, C. Li, W. Yu, D. Chang, Q. Sun, and Y. Jia, Appl. Phys. Lett. **105**, 113105 (2014).

[37] Q. Liu, X. Zhang, L. B. Abdalla, A. Fazzio, and A. Zunger, Nano Lett. **15**, 1222 (2015).

[38] J. Guan, Z. Zhu, and D. Tománek, Phys. Rev. Lett. **113**, 046804 (2014).

[39] A. S. Rodin, A. Carvalho, and A. H. Castro Neto, Phys. Rev. Lett. **112**, 176801 (2014).